SARE: SEMANTIC-AWARE RECONSTRUCTION ERROR FOR GENERALIZABLE AI-GENERATED IMAGE DETECTION

Anonymous authors
Paper under double-blind review

ABSTRACT

Recently, AI-generated image detection has gained increasing attention, as the rapid advancement of image generation technologies has raised serious concerns about their potential misuse. While existing detection methods have achieved promising results, their performance often degrades significantly when facing fake images from unseen, out-of-distribution (OOD) generative models, since they primarily rely on model-specific artifacts and thus overfit to the models used for training. To address this limitation, we propose a novel representation, namely Semantic-Aware Reconstruction Error (SARE), that measures the semantic difference between an image and its caption-guided reconstruction. The key hypothesis behind SARE is that real images, whose captions often fail to fully capture their complex visual content, may undergo noticeable semantic shifts during the caption-guided reconstruction process. In contrast, fake images, which closely align with their captions, show minimal semantic changes. By quantifying these semantic shifts, SARE provides a robust and discriminative feature for detecting fake images across diverse generative models. Additionally, we introduce a fusion module that integrates SARE into the backbone detector via a cross-attention mechanism. Image features attend to semantic representations extracted from SARE, enabling the model to adaptively leverage semantic information. Experimental results demonstrate that the proposed method achieves strong generalization, outperforming existing baselines on benchmarks including GenImage and ForenSynths. We further validate the effectiveness of caption guidance through a detailed analysis of semantic shifts, confirming its ability to enhance detection robustness.

1 INTRODUCTION

In recent years, image generation technologies, such as Generative Adversarial Networks (GANs) (Goodfellow et al., 2014; Zhu et al., 2017; Brock et al., 2019; Karras et al., 2018) and Diffusion Models (DMs) (Ho et al., 2020; Song et al., 2021; Rombach et al., 2022; Nichol et al., 2022), have made remarkable progress, enabling the synthesis of highly realistic images that are often indistinguishable from real images. This realism has raised growing concerns about potential misuse, particularly in generating harmful or deceptive content (Ferreira et al., 2020; Juefei-Xu et al., 2022). To address these risks, developing reliable methods for detecting AI-generated images has become increasingly important.

A common approach in existing detection methods is to train a binary classifier using real and fake images sourced from a finite set of generative models available during training (Bayar & Stamm, 2016; Wang et al., 2020; Liu et al., 2020; Wang et al., 2023). While these detectors typically exhibit strong performance when test images are generated by the same models used during training, their performance often drops significantly in real-world scenarios, where they inevitably encounter fake images from unseen generative models that are not included in the training data (Zhang et al., 2019; Luo et al., 2021; Yan et al., 2023). To ensure robustness in practical deployment, it is essential to develop detection methods that can generalize effectively to such unseen and out-of-distribution (OOD) generative models.

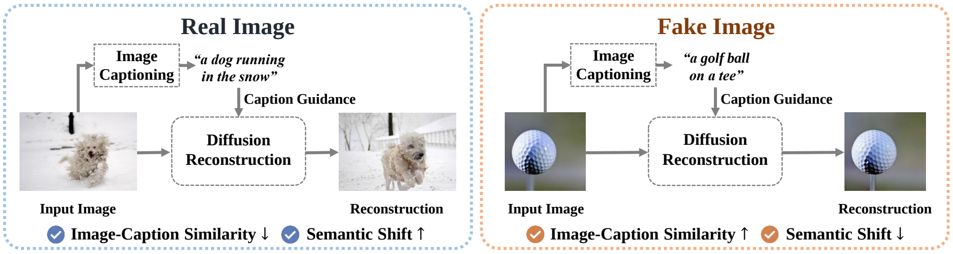

Figure 1: Comparison of caption-guided reconstructions for real and fake images. Real images, whose captions often fail to fully capture their complex visual content, undergo noticeable semantic shifts during caption-guided reconstruction. In contrast, fake images, which align closely with their captions, tend to exhibit minimal semantic changes.

Recent studies have proposed several strategies to address the generalization challenges inherent in generated image detection. These strategies include training methods such as reconstruction-based learning (Wang et al., 2023; Luo et al., 2024; Chu et al., 2025) and data augmentation (Chen et al., 2024), as well as architectural approaches (Ojha et al., 2023; Wu et al., 2023; Tan et al., 2025) that leverage a large pre-trained model like CLIP (Radford et al., 2021). Despite these advances, the robustness of existing methods remains limited, as they primarily focus on identifying visual artifacts introduced during the generative process (Frank et al., 2020; Wang et al., 2020; 2023; Chen et al., 2024). Due to the distinct characteristics of different generative models, such artifacts are inherently model-specific and fail to generalize across diverse models (Luo et al., 2021; Corvi et al., 2023; Ojha et al., 2023). As a result, approaches that rely on these artifacts tend to overfit to the models used for training, which leads to degraded performance in OOD scenarios.

To overcome these limitations, we explore a fundamental property commonly observed in fake images. Prior work (Sha et al., 2023) has shown that the similarity between fake images and captions generated by an image-captioning model is typically higher than that of real images. Real images contain complex, fine-grained details that short captions cannot cover, whereas fake images include only the elements explicitly specified in the user's text prompt. Inspired by this observation, we hypothesize that the relationship between an image and its caption reflects a general characteristic of fake images, providing a robust signal for detection across diverse generative models.

In this paper, we propose Semantic-Aware Reconstruction Error (SARE), a novel representation for detecting AI-generated images that measures the semantic difference between an image and its reconstruction. Specifically, we introduce a caption-guided reconstruction pipeline to effectively leverage the relationship between an image and its caption in the detection process. The key idea is that real images, which often exhibit low similarity to their captions, may undergo noticeable semantic shifts during caption-guided reconstruction. In contrast, fake images, whose content is well captured by their captions, show minimal semantic shifts. As shown in Figure 1, the real image is reconstructed into a noticeably different dog since the caption provides only a coarse description (e.g., "a dog running in the snow") without capturing fine details such as the dog's breed, pose, or background. Conversely, the fake image of a golf ball remains largely unchanged after reconstruction, as its content can be sufficiently described by a simple caption. By capturing these fundamental differences between real and fake images, SARE provides a discriminative and generalizable feature for detecting fake images across diverse generative models. Additionally, we design a fusion module that integrates SARE into the backbone detector via a cross-attention mechanism. The original image features attend to the semantic representations extracted from SARE, allowing the model to adaptively incorporate semantic information.

We validate the effectiveness of SARE through extensive experiments on the GenImage (Zhu et al., 2023) and ForenSynths (Wang et al., 2020) datasets. The proposed framework significantly improves the performance of the backbone model across both seen and unseen generators, achieving the best average results compared to existing detection methods. The results demonstrate the robustness of SARE in OOD scenarios, confirming its strong generalization to fake images from diverse generative models.

2 Related Work

2.1 Detection based on Image Caption

Caption-based detection methods explore the use of image captions as a cue for detecting generated images. DE-FAKE (Sha et al., 2023) finds that generated images tend to align more closely with their captions compared to real images. Based on the observation, it adopts separate encoders for image and caption to exploit the relationship between them. Following this direction, C2P-CLIP (Tan et al., 2025) proposes a method that injects category-level prompts to enhance detection performance. LASTED (Wu et al., 2023) introduces a language-guided contrastive learning framework that leverages textual labels to improve generalization.

2.2 Detection based on Image Reconstruction

Reconstruction-based detection methods utilize a pre-trained diffusion model to reconstruct the input image and analyze the differences between the original and reconstructed images. DIRE (Wang et al., 2023) introduces reconstruction error as the discriminative feature for detection, based on the assumption that fake images can be reconstructed more accurately than real images. To improve efficiency, LaRE (Luo et al., 2024) computes this reconstruction error in the latent space using a single-step denoising process, substantially reducing computational cost while preserving detection performance. DRCT (Chen et al., 2024), rather than relying on reconstruction error, treats reconstructed images as hard samples and adopts a contrastive learning framework to facilitate discriminative feature learning. FakeInversion (Cazenavette et al., 2024) not only exploits the reconstructed images but also incorporates additional feature maps derived from caption-conditioned DDIM inversion (Song et al., 2021), where captions are mainly employed to stabilize the inversion and reconstruction process. In contrast, our method SARE explicitly leverages the relationship between an image and its caption. Motivated by the observation that fake images tend to exhibit higher similarity to their captions than real images, SARE quantifies the semantic difference between the image and its caption-guided reconstruction. This semantic-aware discrepancy serves as a robust detection signal, enabling SARE to generalize effectively across diverse generative models.

3 Proposed Method

3.1 Motivation

Existing methods (Frank et al., 2020; Wang et al., 2020; 2023; Chen et al., 2024) for detecting fake images primarily rely on visual artifacts or traces left by the generative models. A representative example is DIRE (Wang et al., 2023), which reconstructs the input image with a pre-trained diffusion model and leverages the pixel-wise reconstruction error as a discriminative feature for classification. It is based on the assumption that fake images exhibit smaller reconstruction errors than real images, as both the original and reconstructed images belong to the same generative distribution and thus share similar visual patterns. However, our empirical observation suggests that this assumption often does not hold in OOD scenarios, where fake images are synthesized by unseen generators that were not available during training. As shown in Figure 2, when Stable Diffusion v1.4 (Rombach et al., 2022) is used for reconstruction, fake images from unseen models such as ADM (Dhariwal & Nichol, 2021) or BigGAN (Brock et al., 2019) produce much larger reconstruction errors, even exceeding those of real images. This implies that diverse generative models,

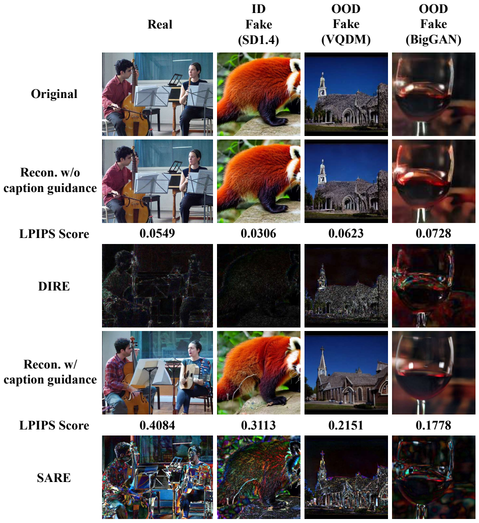

Figure 2: Examples from the GenImage dataset (Zhu et al., 2023) and their corresponding DIREs (Wang et al., 2023), SAREs, and LPIPS scores. Images are reconstructed using Stable Diffusion v1.4, and the pixel values of the DIREs and SAREs are scaled by 2 for clearer visualization.

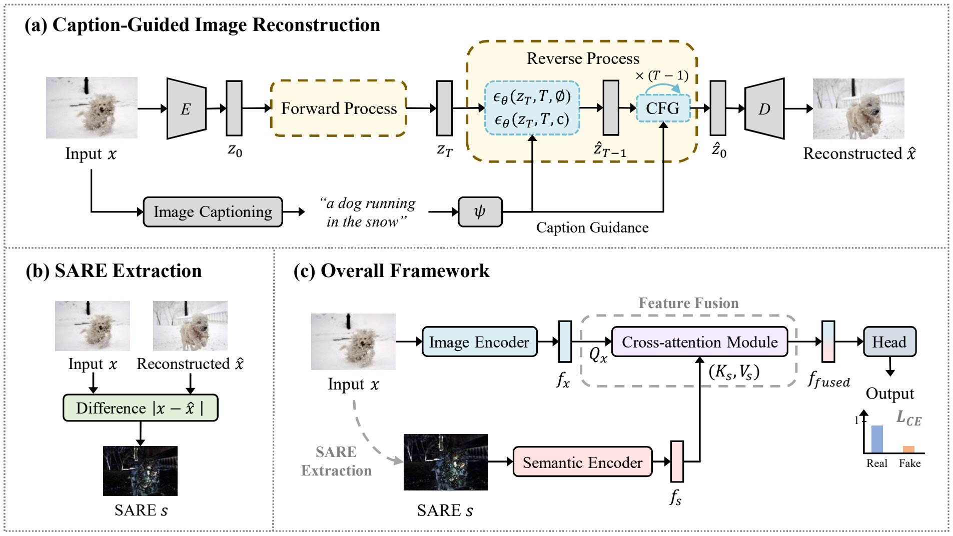

Figure 3: Overview of the SARE framework. Our method reconstructs the input image conditioned on its caption using the Stable Diffusion model with classifier-free guidance. SARE is computed as the difference between the input and reconstructed image, and is incorporated into the detection process through a cross-attention module that leverages image features as queries and SARE features as keys and values. The pixel values of the SARE are scaled by 2 for clearer visualization.

including the reconstruction model and unseen generators, exhibit distinctive characteristics and traces. From this observation, we suggest that methods relying on visual artifacts from a specific generation process may struggle to generalize in OOD scenarios. This limitation highlights the need for more generalizable detection cues that can perform reliably across diverse generative models.

3.2 Semantic-aware Reconstruction Error

We propose Semantic-Aware Reconstruction Error (SARE), a novel detection feature designed to enhance generalization in AI-generated image detection. The hypothesis of SARE is that the relationship between an image and its caption may reflect fundamental differences between real and fake images, and thus serve as a generalizable detection cue. SARE aims to effectively leverage this property by introducing a caption-guided reconstruction framework. The framework consists of three main steps: (1) image captioning, (2) caption-guided image reconstruction, and (3) SARE extraction.

Image Captioning For a given image x, we utilize a pre-trained image captioning model to generate a descriptive caption C. This caption C is used as the text condition for the subsequent reconstruction process.

Caption-guided Image Reconstruction Given the caption C, we reconstruct the input image x by using a pre-trained text-conditional diffusion model. Specifically, we leverage the Stable Diffusion model (Rombach et al., 2022) with classifier-free guidance (Ho & Salimans, 2021). The input image x is first encoded into a latent representation z_0 using the Variational Autoencoder (VAE) encoder (Kingma & Welling, 2014). The forward process then adds Gaussian noise to z_0 following a predefined noise schedule. The noisy latent at a given timestep t is computed as:

$$z_t = \sqrt{\bar{\alpha}_t} z_0 + \sqrt{1 - \bar{\alpha}_t}\epsilon, \tag{1}$$

where $\epsilon \sim \mathcal{N}(0, \mathbf{I})$, and $\bar{\alpha}_t = \prod_{s=1}^{t} \alpha_s$. The *strength* parameter determines the amount of noise added during reconstruction. The number of forward diffusion steps is set to $T = \lfloor \textit{strength} \times T_{\max} \rfloor$, where $T_{\max}$ is the total number of diffusion steps.

Starting from the noisy latent z_T, the reverse process aims to obtain $\hat{z}_0$ through an iterative denoising process conditioned on the caption C. At each denoising step, the noise prediction network

$\epsilon_\theta(z_t, t, c)$ estimates the noise ϵ, where $c = \psi(C)$ denotes the caption embedding obtained from the CLIP text encoder (Radford et al., 2021). We adopt classifier-free guidance, which combines the conditional and unconditional noise predictions as follows:

$$\epsilon_\theta(z_t, t, c, \varnothing) = w\epsilon_\theta(z_t, t, c) + (1-w)\epsilon_\theta(z_t, t, \varnothing), \tag{2}$$

where w is the guidance scale and $\varnothing = \psi(\text{``''})$ denotes the null text embedding. The denoising process using DDIM sampling (Song et al., 2021) can be represented by:

$$z_{t-1} = \sqrt{\alpha_{t-1}} \frac{z_t - \sqrt{1-\alpha_t}\,\epsilon_\theta(z_t, t, c, \varnothing)}{\sqrt{\alpha_t}} + \sqrt{1-\alpha_{t-1}}\epsilon_t, \tag{3}$$

where $\alpha_{t-1} = \frac{\bar{\alpha}_{t-1}}{\bar{\alpha}_t}$ and $\epsilon \sim \mathcal{N}(0, \mathbf{I})$, for $t = T, ..., 1$. After T denoising steps, the final latent $\hat{z}_0$ is obtained and decoded by the VAE decoder to produce the reconstructed image $\hat{x}$.

SARE Extraction Once we obtain the original image x and the reconstructed image $\hat{x}$, we compute the SARE by measuring the difference between the two images. SARE is defined as follows:

$$\text{SARE}(x, \hat{x}) = |x - \hat{x}|, \tag{4}$$

where $|\cdot|$ denotes the absolute value. SARE quantifies the semantic changes introduced during the caption-guided reconstruction process. Since real images often contain complex visual details that cannot be fully reflected in their captions, their reconstructions result in noticeable semantic shifts. In contrast, fake images typically align closely with their captions and therefore tend to undergo minimal semantic changes. By capturing these differences between real and fake images, SARE can serve as a discriminative feature for robust detection across diverse generative models.

3.3 Fusion Module

We propose a fusion module to effectively integrate SARE into the detection process. Given an input image x and its corresponding SARE s, we extract the image feature f_x and the semantic feature f_s using the image encoder E_x and the semantic encoder E_s, respectively:

$$f_x = E_x(x), \ f_s = E_s(s). \tag{5}$$

To obtain the fused feature f_{fused}, we employ a cross-attention mechanism by leveraging f_x for query and f_s for key and value as follows:

$$\begin{gathered} Q_x = f_x W_Q, \ K_s = f_s W_K, \ V_s = f_s W_V, \\ f_{fused} = CrossAttn(Q_x, K_s, V_s), \end{gathered} \tag{6}$$

where W_Q, W_K, and W_V are the linear projections for the query, key, and value, respectively. This fused representation allows the model to incorporate semantic information as an additional cue. Subsequently, f_{fused} is passed through a fully connected layer that serves as the classification head, and the model is trained using binary cross-entropy loss.

4 Experiment

4.1 Experimental Settings

Datasets and Evaluation Metrics We evaluated the performance of detection models using the GenImage (Zhu et al., 2023) dataset, which is divided into 8 subsets. Each subset consists of real images from ImageNet Deng et al. (2009) and fake images synthesized by a single generative model. The generative models are Midjourney (MJ) (Mid, 2022), Stable Diffusion v1.4&v1.5 (SDv1.4&v1.5) (Rombach et al., 2022), ADM (Dhariwal & Nichol, 2021), GLIDE (Nichol et al., 2022), Wukong (Wuk, 2022), VQDM (Gu et al., 2022), and BigGAN (Brock et al., 2019). We used the training split from the SDv1.4 subset for training, and the test splits from all subsets for evaluation. For cross-dataset evaluation, we trained the models on the SDv1.4 subset of GenImage and evaluated them on the ForenSynths (Wang et al., 2020) test set. The ForenSynths test set contains 11 subsets, where each subset comprises real images from the training data of a specific generative model and fake images produced by that model. The generative models in ForenSynths include

Method	MJ	SDv1.4	SDv1.5	ADM	GLIDE	Wukong	VQDM	BigGAN	Avg ACC.(%)
GramNet	73.32	96.73	96.55	51.73	58.85	91.19	57.05	48.63	71.76
Conv-B	84.59	**100.00**	**99.91**	52.86	57.14	**99.88**	58.77	50.01	75.40
UnivFD	89.56	96.94	96.56	57.20	71.12	95.03	68.67	57.83	79.11
DIRE	51.03	99.96	**99.91**	51.78	59.26	99.79	50.18	50.88	70.35
DE-FAKE	85.55	97.93	97.82	53.53	65.28	91.57	55.98	49.16	74.60
DRCT	**90.89**	94.75	94.28	78.54	87.52	94.58	90.12	79.76	88.81
SARE (ours)	90.32	97.21	97.04	**84.47**	**93.55**	97.05	**93.66**	**92.05**	**93.17**

Table 1: Accuracy (ACC, %) comparisons of different detectors on the GenImage dataset (Zhu et al., 2023). All methods are trained on the SDv1.4 subset and evaluated across 8 subsets. The best and second-best results are indicated in **bold** and underlined, respectively.

Method	MJ	SDv1.4	SDv1.5	ADM	GLIDE	Wukong	VQDM	BigGAN	Avg AUC.(%)
GramNet	91.54	99.56	99.49	69.87	83.52	98.10	78.40	39.36	82.48
Conv-B	**99.54**	**100.00**	**99.94**	90.10	96.72	**100.00**	93.82	86.61	95.84
UnivFD	97.54	99.57	99.51	73.09	89.46	98.99	87.53	79.19	90.61
DIRE	78.65	**100.00**	**99.94**	71.45	90.42	99.99	62.49	61.12	83.01
DE-FAKE	97.13	99.81	99.80	70.95	89.26	98.52	78.48	57.60	86.44
DRCT	96.91	99.64	99.52	88.47	94.61	99.42	96.44	90.30	95.66
SARE (ours)	96.83	99.94	99.93	**94.87**	**98.00**	99.83	**98.31**	**97.51**	**98.15**

Table 2: AUC (%) comparisons of different detectors on the GenImage dataset (Zhu et al., 2023). All methods are trained on the SDv1.4 subset and evaluated across 8 subsets. The best and second-best results are indicated in **bold** and underlined, respectively.

ProGAN (Karras et al., 2018), StyleGAN (Karras et al., 2019), BigGAN (Brock et al., 2019), CycleGAN (Zhu et al., 2017), StarGAN (Choi et al., 2018), GauGAN (Park et al., 2019), CRN (Chen & Koltun, 2017), IMLE (Li et al., 2019), SITD (Chen et al., 2018), SAN (Dai et al., 2019), and Deepfake (Rossler et al., 2019). For evaluation metrics, we employed accuracy (ACC) and the Area Under the ROC curve (AUC). Accuracy was computed with a fixed threshold of 0.5, following the baseline settings Wang et al. (2023); Chen et al. (2024).

Implementation Details To obtain reconstructed images for SARE and for the baseline models DIRE (Wang et al., 2023) and DRCT (Chen et al., 2024), we used SDv1 as the reconstruction model. For SARE, captions were generated using a pre-trained BLIP model (Li et al., 2022). Each caption was used to guide the reconstruction process, where we set the strength parameter to 0.5, the guidance scale to 7.5, and the maximum number of diffusion steps to 50. We adopted DRCT as the backbone detector, which utilizes CLIP:ViT-L/14 (Radford et al., 2021) as the image encoder. For the semantic encoder, we employed a ResNet50 model (He et al., 2016). During training, we applied random cropping and several augmentations, including horizontal flipping, Gaussian noise injection, Gaussian blurring, random rotation, JPEG compression with random quality, random scaling, grid dropout, and brightness and contrast adjustments. At test time, images were center-cropped. All models were designed to take input images of size 224 × 224. For SARE extraction, images were resized to 512 on the longer side before reconstruction, and the resulting SARE representations were fed into the encoder at a size of 224 × 224. We trained our proposed model for 17 epochs with a batch size of 512 and used the AdamW optimizer (Loshchilov & Hutter, 2019) with an initial learning rate of 1×10^{-4}.

4.2 Comparisons to Existing Detectors

Tables 1 and 2 report the accuracies and AUC scores of different detection methods on the GenImage dataset. We compared our method with several detectors, including GramNet Liu et al. (2020), Conv-B (Liu et al., 2022), UnivFD (Ojha et al., 2023), DIRE, DE-FAKE (Sha et al., 2023), and DRCT. All models were trained on the SDv1.4 subset. For DE-FAKE, we used BLIP for caption-

Method	Pro- GAN	Style- GAN	Big- GAN	Cycle- GAN	Star- GAN	Gau- GAN	CRN	IMLE	SITD	SAN	Deep- Fake	Avg ACC.(%)
GramNet	49.20	48.57	49.73	48.91	49.05	48.70	47.59	47.50	65.56	57.99	58.02	51.89
Conv-B	54.66	50.47	52.50	50.03	49.47	50.19	**49.94**	52.50	62.5	66.44	**80.19**	56.26
UnivFD	67.97	53.92	68.47	67.73	**79.94**	56.21	38.04	54.64	63.89	65.53	60.56	61.54
DIRE	50.06	50.03	49.88	49.94	50.05	49.97	49.44	49.59	53.89	73.29	52.58	52.61
DE-FAKE	51.20	48.39	52.88	51.49	63.81	49.02	49.46	47.31	53.89	65.30	51.77	53.14
DRCT	74.59	67.41	83.10	**92.40**	62.23	78.89	41.67	51.86	**66.11**	79.45	55.78	68.50
SARE (ours)	**84.44**	**76.32**	**83.17**	90.24	59.58	**81.28**	46.6	**60.94**	61.39	**85.16**	51.54	**70.97**

Table 3: Accuracy (ACC, %) comparisons of different detectors under cross-dataset evaluation. All detectors are trained on the SDv1.4 subset of the GenImage dataset (Zhu et al., 2023) and evaluated on the ForenSynths test set (Wang et al., 2020). The best and second-best results are indicated in **bold** and underlined, respectively.

Method	Pro- GAN	Style- GAN	Big- GAN	Cycle- GAN	Star- GAN	Gau- GAN	CRN	IMLE	SITD	SAN	Deep- Fake	Avg AUC.(%)
GramNet	49.08	45.59	50.76	55.73	48.46	34.39	49.90	39.23	75.14	70.14	63.88	52.94
Conv-B	75.66	74.59	77.46	53.58	38.18	62.23	44.21	**85.55**	86.54	**98.62**	**87.58**	71.29
UnivFD	81.38	64.79	84.46	93.63	89.31	80.03	29.51	57.22	74.75	75.07	67.96	72.56
DIRE	55.64	52.37	45.25	47.64	51.94	45.38	43.86	62.73	**93.95**	98.44	84.34	61.96
DE-FAKE	55.74	46.53	70.09	76.11	71.15	43.10	**51.76**	46.21	51.93	77.38	51.11	58.28
DRCT	89.35	75.73	**92.74**	**98.28**	**95.93**	88.23	29.35	68.55	79.46	88.76	80.01	79.67
SARE (ours)	**93.45**	**87.05**	92.10	95.83	94.80	**90.43**	47.73	79.10	77.70	92.52	77.68	**84.40**

Table 4: AUC (%) comparisons of different detectors under cross-dataset evaluation. All detectors are trained on the SDv1.4 subset of the GenImage dataset (Zhu et al., 2023) and evaluated on the ForenSynths test set (Wang et al., 2020). The best and second-best results are indicated in **bold** and underlined, respectively.

ing, following the configuration described in the original paper. The results show that compared to DRCT, our method improves the average accuracy by 4.36%, and the average AUC by 2.49%, which indicates that integrating SARE effectively enhances the detection performance. Notably, our method achieves the highest average accuracy of 93.17% and AUC of 98.15%, outperforming all other detection approaches. While all the detectors show strong performance on SDv1.4, SDv1.5, and Wukong subsets, their performance tends to degrade significantly on other subsets like ADM, GLIDE, VQDM, and the non-diffusion model BigGAN. Our method maintains consistently high performance across all subsets, demonstrating robust generalization to diverse OOD generative models. Moreover, the proposed method outperforms DE-FAKE, suggesting that SARE leverages the relationship between an image and its caption more effectively than directly comparing image and caption embeddings obtained from CLIP.

4.3 Cross-dataset Evaluation

To further assess the generalization ability of the detection methods, we conducted a cross-dataset evaluation. All detectors were trained on the SDv1.4 subset of the GenImage dataset and evaluated on the ForenSynths test set. Table 3 and Table 4 report the accuracy and AUC score of each method on this test set. Our method shows strong performance across diverse generative models, yielding an average accuracy of 70.97% and an average AUC of 84.40%, which are the highest among all detectors. These results highlight the effectiveness of our method in OOD scenarios, demonstrating its robust generalization to fake images from unseen generative models.

4.4 Semantic Shift Analysis

Quantitative Results To validate the core assumption that real images undergo larger semantic shifts than fake images, we measured the perceptual distance between an image x and its reconstruction $\hat{x}$ using the Learned Perceptual Image Patch Similarity (LPIPS) (Zhang et al., 2018) metric. Figure 4a summarizes the average LPIPS scores for real and fake images in each subset of the GenImage dataset under two conditions: (1) reconstruction without caption guidance, and (2)

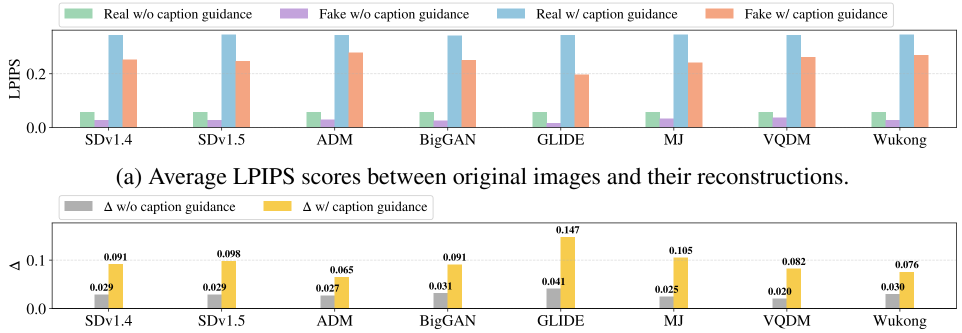

(a) Average LPIPS scores between original images and their reconstructions.

(b) Δ values measuring the LPIPS score gap between real and fake images.

Figure 4: Semantic shift analysis based on LPIPS scores (Zhang et al., 2018). Higher scores indicate lower similarity between the original and reconstructed images. Images are reconstructed under two conditions: with and without caption guidance.

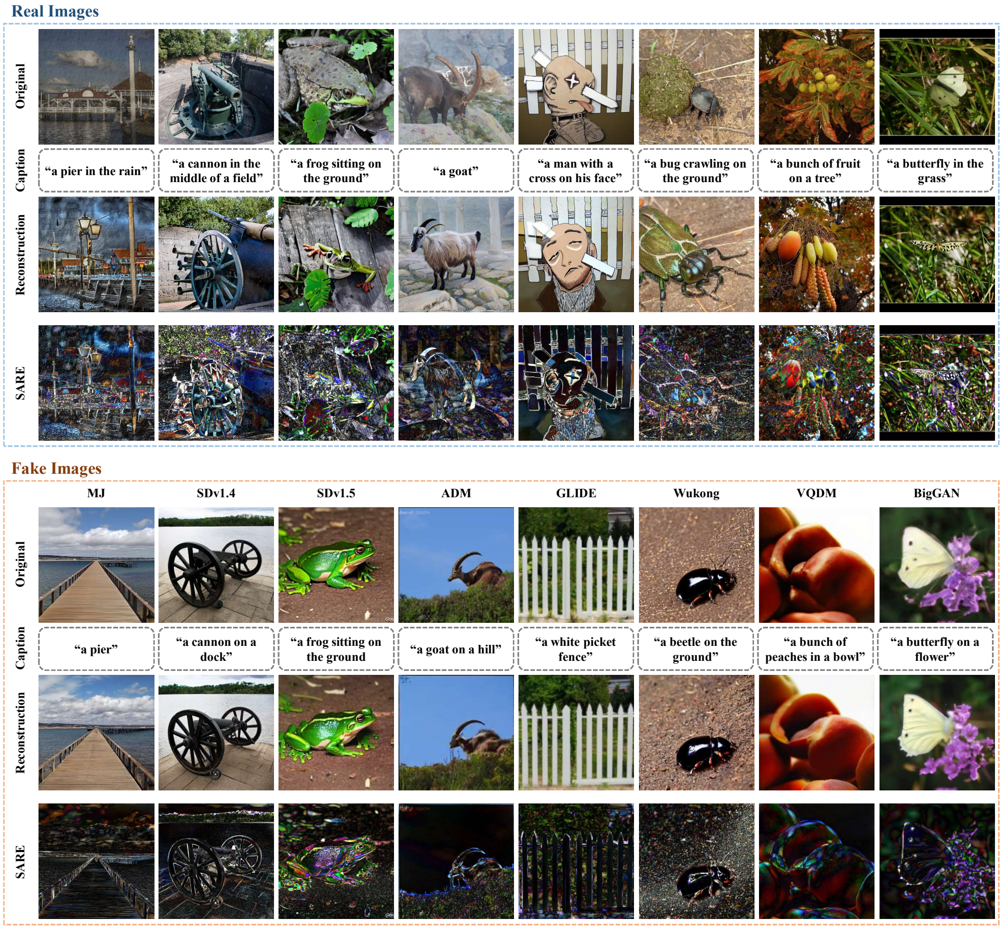
Real Images
Original
Caption
Reconstruction
SARE
"a pier in the rain"
"a cannon in the middle of a field"
"a frog sitting on the ground"
"a goat"
"a man with a cross on his face"
"a bug crawling on the ground"
"a bunch of fruit on a tree"
"a butterfly in the grass"
Fake Images
MJ
SDv1.4
SDv1.5
ADM
GLIDE
Wukong
VQDM
BigGAN
"a pier"
"a cannon on a dock"
"a frog sitting on the ground"
"a goat on a hill"
"a white picket fence"
"a beetle on the ground"
"a bunch of peaches in a bowl"
"a butterfly on a flower"

Figure 5: Real and fake images from the GenImage dataset (Zhu et al., 2023) with their captions generated by a pre-trained BLIP (Li et al., 2022), the corresponding reconstructions, and SAREs.

reconstruction with caption guidance. While real images consistently exhibit higher LPIPS scores than fake images in both settings, the gap between real and fake images is substantially larger when caption guidance is applied. To quantify this gap, we define Δ as follows:

$$\Delta = \mathbb{E}_{x\sim\mathcal{D}_{\text{real}}}[LPIPS(x,\hat{x})] - \mathbb{E}_{x\sim\mathcal{D}_{\text{fake}}}[LPIPS(x,\hat{x})]. \tag{7}$$

Method	Image Captioning	Avg ACC.(%)	Avg AUC.(%)
DRCT	-	88.81	95.66
SARE (ours)	BLIP	**93.17**	**98.15**
	LLaVA-NeXT	92.51	97.95

Table 5: Ablation study on the influence of image captioning models on the GenImage dataset (Zhu et al., 2023).

Method	w	Avg ACC.(%)	Avg AUC.(%)
DRCT	-	88.81	95.66
SARE (ours)	2.5	93.15	**98.24**
	7.5	**93.17**	98.15
	12.5	93.04	98.13

Table 6: Ablation study on the guidance scale w conducted on the GenImage dataset (Zhu et al., 2023).

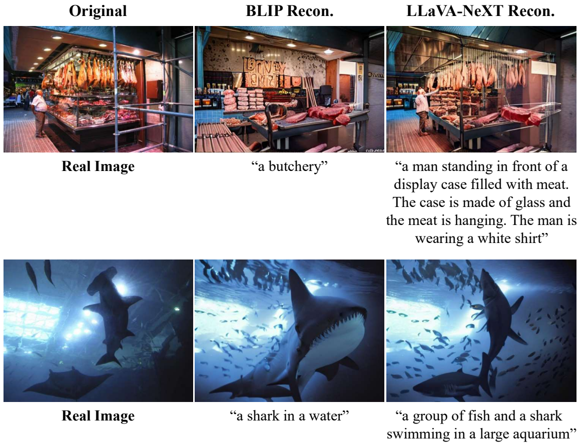
Original
BLIP Recon.
LLaVA-NeXT Recon.
Real Image
"a butchery"
"a man standing in front of a display case filled with meat. The case is made of glass and the meat is hanging. The man is wearing a white shirt"
Real Image
"a shark in a water"
"a group of fish and a shark swimming in a large aquarium"

Figure 6: Real images from the GenImage dataset (Zhu et al., 2023) with captions from BLIP (Li et al., 2022) and LLaVA-NeXT (Liu et al., 2024), and their reconstructions.

As shown in Figure 4b, Δ is relatively small without caption guidance, but increases significantly in all subsets when caption guidance is used. These results suggest that the semantic difference between an image and its caption-guided reconstruction may serve as a more discriminative feature for detection, thereby leading to improved performance across diverse generative models.

Qualitative Results and Visualizations Figure 5 presents qualitative examples of real and fake images from the GenImage dataset and their caption-guided reconstructions, where captions were generated using a pre-trained BLIP. In GenImage, real images are sourced from ImageNet, while fake images are synthesized by generative models using ImageNet class labels as text prompts. For a fair comparison, we visualize real and fake images from the same ImageNet class label along with their reconstructions. The results show that real images tend to undergo larger semantic shifts than fake images during the caption-guided reconstruction process.

4.5 Ablation Study

Influence of Image Captioning models To evaluate the impact of different image captioning models on detection performance, we conducted an ablation study using captions generated by pre-trained BLIP and LLaVA-NeXT-8B (Liu et al., 2024) on the GenImage dataset. As shown in Table 5, SARE demonstrates strong performance with both captioning models, but BLIP consistently achieves higher accuracy and AUC. To further examine this difference, Figure 6 visualizes real images from GenImage and their reconstructions guided by captions from the two models. BLIP tends to generate concise captions such as "a butchery", which do not fully capture fine details like "a man in a white shirt" or "hanging meat". As a result, the reconstructed images differ significantly from the original, leading to noticeable semantic shifts. In contrast, LLaVA-NeXT provides more detailed descriptions that include such elements, yielding reconstructions that remain relatively close to the input image and thus exhibit smaller semantic changes. These observations suggest that BLIP's coarse captions induce larger semantic shifts in real images, thereby enhancing the effectiveness of SARE in distinguishing real from fake images. A more detailed analysis of captioning models is presented in Appendix A.

Influence of Guidance Scale We investigated the impact of the guidance scale w on detection performance within the caption-guided reconstruction framework. Table 6 presents the accuracy and AUC results on the GenImage dataset for different guidance scale values. The results show that incorporating SARE consistently improves the performance over the baseline across all settings. Notably, the best accuracy is achieved at $w = 7.5$ (93.17%), whereas the highest AUC is observed at $w = 2.5$ (98.24%).

5 Conclusion

In this paper, we introduced a novel representation for AI-generated image detection, termed Semantic-Aware Reconstruction Error (SARE), that quantifies the semantic difference between an image and its caption-guided reconstruction. By effectively leveraging the relationship between an image and its caption, SARE provided a discriminative and generalizable feature for detecting fake images across diverse generative models. Our experimental results demonstrated that SARE significantly improved detection performance in both ID and OOD settings, surpassing existing baselines.

References

Midjourney. `https://www.midjourney.com/home`, 2022.

Wukong. `https://xihe.mindspore.cn/modelzoo/wukong`, 2022.

Belhassen Bayar and Matthew C Stamm. A deep learning approach to universal image manipulation detection using a new convolutional layer. In *Proceedings of the ACM Workshop on Information Hiding and Multimedia Security*, pp. 5–10, 2016.

Andrew Brock, Jeff Donahue, and Karen Simonyan. Large scale GAN training for high fidelity natural image synthesis. In *International Conference on Learning Representations*, 2019.

George Cazenavette, Avneesh Sud, Thomas Leung, and Ben Usman. Fakeinversion: Learning to detect images from unseen text-to-image models by inverting stable diffusion. In *Proceedings of the IEEE/CVF Conference on Computer Vision and Pattern Recognition*, pp. 10759–10769, 2024.

Baoying Chen, Jishen Zeng, Jianquan Yang, and Rui Yang. Drct: Diffusion reconstruction contrastive training towards universal detection of diffusion generated images. In *International Conference on Machine Learning*, 2024.

Chen Chen, Qifeng Chen, Jia Xu, and Vladlen Koltun. Learning to see in the dark. In *Proceedings of the IEEE/CVF Conference on Computer Vision and Pattern Recognition*, pp. 3291–3300, 2018.

Qifeng Chen and Vladlen Koltun. Photographic image synthesis with cascaded refinement networks. In *Proceedings of the IEEE International Conference on Computer Vision*, pp. 1511–1520, 2017.

Yunjey Choi, Minje Choi, Munyoung Kim, Jung-Woo Ha, Sunghun Kim, and Jaegul Choo. Stargan: Unified generative adversarial networks for multi-domain image-to-image translation. In *Proceedings of the IEEE/CVF Conference on Computer Vision and Pattern Recognition*, pp. 8789–8797, 2018.

Beilin Chu, Xuan Xu, Xin Wang, Yufei Zhang, Weike You, and Linna Zhou. Fire: Robust detection of diffusion-generated images via frequency-guided reconstruction error. In *Proceedings of the IEEE/CVF Conference on Computer Vision and Pattern Recognition*, pp. 12830–12839, 2025.

Riccardo Corvi, Davide Cozzolino, Giada Zingarini, Giovanni Poggi, Koki Nagano, and Luisa Verdoliva. On the detection of synthetic images generated by diffusion models. In *IEEE International Conference on Acoustics, Speech and Signal Processing*, pp. 1–5, 2023.

Tao Dai, Jianrui Cai, Yongbing Zhang, Shu-Tao Xia, and Lei Zhang. Second-order attention network for single image super-resolution. In *Proceedings of the IEEE/CVF Conference on Computer Vision and Pattern Recognition*, pp. 11065–11074, 2019.

Jia Deng, Wei Dong, Richard Socher, Li-Jia Li, Kai Li, and Li Fei-Fei. Imagenet: A large-scale hierarchical image database. In *IEEE Conference on Computer Vision and Pattern Recognition*, pp. 248–255, 2009.

Prafulla Dhariwal and Alexander Nichol. Diffusion models beat gans on image synthesis. *Advances in Neural Information Processing Systems*, 34:8780–8794, 2021.

William D Ferreira, Cristiane BR Ferreira, Gelson da Cruz Júnior, and Fabrizzio Soares. A review of digital image forensics. *Computers & Electrical Engineering*, 85:106685, 2020.

Joel Frank, Thorsten Eisenhofer, Lea Schönherr, Asja Fischer, Dorothea Kolossa, and Thorsten Holz. Leveraging frequency analysis for deep fake image recognition. In *International Conference on Machine Learning*, pp. 3247–3258. PMLR, 2020.

Ian J Goodfellow, Jean Pouget-Abadie, Mehdi Mirza, Bing Xu, David Warde-Farley, Sherjil Ozair, Aaron Courville, and Yoshua Bengio. Generative adversarial nets. *Advances in Neural Information Processing Systems*, 27, 2014.

Shuyang Gu, Dong Chen, Jianmin Bao, Fang Wen, Bo Zhang, Dongdong Chen, Lu Yuan, and Baining Guo. Vector quantized diffusion model for text-to-image synthesis. In *Proceedings of the IEEE/CVF Conference on Computer Vision and Pattern Recognition*, pp. 10696–10706, 2022.

Kaiming He, Xiangyu Zhang, Shaoqing Ren, and Jian Sun. Deep residual learning for image recognition. In *Proceedings of the IEEE Conference on Computer Vision and Pattern Recognition*, pp. 770–778, 2016.

Jonathan Ho and Tim Salimans. Classifier-free diffusion guidance. In *NeurIPS 2021 Workshop on Deep Generative Models and Downstream Applications*, 2021.

Jonathan Ho, Ajay Jain, and Pieter Abbeel. Denoising diffusion probabilistic models. *Advances in Neural Information Processing Systems*, 33:6840–6851, 2020.

Felix Juefei-Xu, Run Wang, Yihao Huang, Qing Guo, Lei Ma, and Yang Liu. Countering malicious deepfakes: Survey, battleground, and horizon. *International Journal of Computer Vision*, 130(7): 1678–1734, 2022.

Tero Karras, Timo Aila, Samuli Laine, and Jaakko Lehtinen. Progressive growing of GANs for improved quality, stability, and variation. In *International Conference on Learning Representations*, 2018.

Tero Karras, Samuli Laine, and Timo Aila. A style-based generator architecture for generative adversarial networks. In *Proceedings of the IEEE/CVF Conference on Computer Vision and Pattern Recognition*, pp. 4401–4410, 2019.

Diederik P. Kingma and Max Welling. Auto-Encoding Variational Bayes. In *International Conference on Learning Representations*, 2014.

Junnan Li, Dongxu Li, Caiming Xiong, and Steven Hoi. Blip: Bootstrapping language-image pre-training for unified vision-language understanding and generation. In *International Conference on Machine Learning*, pp. 12888–12900. PMLR, 2022.

Ke Li, Tianhao Zhang, and Jitendra Malik. Diverse image synthesis from semantic layouts via conditional imle. In *Proceedings of the IEEE/CVF International Conference on Computer Vision*, pp. 4220–4229, 2019.

Haotian Liu, Chunyuan Li, Yuheng Li, Bo Li, Yuanhan Zhang, Sheng Shen, and Yong Jae Lee. Llavanext: Improved reasoning, ocr, and world knowledge, 2024.

Zhengzhe Liu, Xiaojuan Qi, and Philip HS Torr. Global texture enhancement for fake face detection in the wild. In *Proceedings of the IEEE/CVF Conference on Computer Vision and Pattern Recognition*, pp. 8060–8069, 2020.

Zhuang Liu, Hanzi Mao, Chao-Yuan Wu, Christoph Feichtenhofer, Trevor Darrell, and Saining Xie. A convnet for the 2020s. In *Proceedings of the IEEE/CVF Conference on Computer Vision and Pattern Recognition*, pp. 11976–11986, 2022.

Ilya Loshchilov and Frank Hutter. Decoupled weight decay regularization. In *International Conference on Learning Representations*, 2019.

Yuchen Luo, Yong Zhang, Junchi Yan, and Wei Liu. Generalizing face forgery detection with high-frequency features. In *Proceedings of the IEEE/CVF Conference on Computer Vision and Pattern Recognition*, pp. 16317–16326, 2021.

Yunpeng Luo, Junlong Du, Ke Yan, and Shouhong Ding. Lareˆ 2: Latent reconstruction error based method for diffusion-generated image detection. In *Proceedings of the IEEE/CVF Conference on Computer Vision and Pattern Recognition*, pp. 17006–17015, 2024.

Alexander Quinn Nichol, Prafulla Dhariwal, Aditya Ramesh, Pranav Shyam, Pamela Mishkin, Bob Mcgrew, Ilya Sutskever, and Mark Chen. Glide: Towards photorealistic image generation and editing with text-guided diffusion models. In *International Conference on Machine Learning*, pp. 16784–16804. PMLR, 2022.

Utkarsh Ojha, Yuheng Li, and Yong Jae Lee. Towards universal fake image detectors that generalize across generative models. In *Proceedings of the IEEE/CVF Conference on Computer Vision and Pattern Recognition*, pp. 24480–24489, 2023.

Taesung Park, Ming-Yu Liu, Ting-Chun Wang, and Jun-Yan Zhu. Semantic image synthesis with spatially-adaptive normalization. In *Proceedings of the IEEE/CVF Conference on Computer Vision and Pattern Recognition*, pp. 2337–2346, 2019.

Alec Radford, Jong Wook Kim, Chris Hallacy, Aditya Ramesh, Gabriel Goh, Sandhini Agarwal, Girish Sastry, Amanda Askell, Pamela Mishkin, Jack Clark, et al. Learning transferable visual models from natural language supervision. In *International Conference on Machine Learning*, pp. 8748–8763. PMLR, 2021.

Robin Rombach, Andreas Blattmann, Dominik Lorenz, Patrick Esser, and Björn Ommer. High-resolution image synthesis with latent diffusion models. In *Proceedings of the IEEE/CVF Conference on Computer Vision and Pattern Recognition*, pp. 10684–10695, 2022.

Andreas Rossler, Davide Cozzolino, Luisa Verdoliva, Christian Riess, Justus Thies, and Matthias Nießner. Faceforensics++: Learning to detect manipulated facial images. In *Proceedings of the IEEE/CVF International Conference on Computer Vision*, pp. 1–11, 2019.

Zeyang Sha, Zheng Li, Ning Yu, and Yang Zhang. De-fake: Detection and attribution of fake images generated by text-to-image generation models. In *Proceedings of the 2023 ACM SIGSAC Conference on Computer and Communications Security*, pp. 3418–3432, 2023.

Jiaming Song, Chenlin Meng, and Stefano Ermon. Denoising diffusion implicit models. In *International Conference on Learning Representations*, 2021.

Chuangchuang Tan, Yao Zhao, Shikui Wei, Guanghua Gu, Ping Liu, and Yunchao Wei. Rethinking the up-sampling operations in cnn-based generative network for generalizable deepfake detection. In *Proceedings of the IEEE/CVF Conference on Computer Vision and Pattern Recognition*, pp. 28130–28139, 2024.

Chuangchuang Tan, Renshuai Tao, Huan Liu, Guanghua Gu, Baoyuan Wu, Yao Zhao, and Yunchao Wei. C2p-clip: Injecting category common prompt in clip to enhance generalization in deepfake detection. In *Proceedings of the AAAI Conference on Artificial Intelligence*, volume 39, pp. 7184–7192, 2025.

Sheng-Yu Wang, Oliver Wang, Richard Zhang, Andrew Owens, and Alexei A Efros. Cnn-generated images are surprisingly easy to spot... for now. In *Proceedings of the IEEE/CVF Conference on Computer Vision and Pattern Recognition*, pp. 8695–8704, 2020.

Zhendong Wang, Jianmin Bao, Wengang Zhou, Weilun Wang, Hezhen Hu, Hong Chen, and Houqiang Li. Dire for diffusion-generated image detection. In *Proceedings of the IEEE/CVF International Conference on Computer Vision*, pp. 22445–22455, 2023.

Haiwei Wu, Jiantao Zhou, and Shile Zhang. Generalizable synthetic image detection via language-guided contrastive learning. *arXiv preprint arXiv:2305.13800*, 2023.

Shilin Yan, Ouxiang Li, Jiayin Cai, Yanbin Hao, Xiaolong Jiang, Yao Hu, and Weidi Xie. A sanity check for AI-generated image detection. In *International Conference on Learning Representations*, 2025.

Zhiyuan Yan, Yong Zhang, Yanbo Fan, and Baoyuan Wu. Ucf: Uncovering common features for generalizable deepfake detection. In *Proceedings of the IEEE/CVF International Conference on Computer Vision*, pp. 22412–22423, 2023.

Richard Zhang, Phillip Isola, Alexei A Efros, Eli Shechtman, and Oliver Wang. The unreasonable effectiveness of deep features as a perceptual metric. In *Proceedings of the IEEE/CVF Conference on Computer Vision and Pattern Recognition*, pp. 586–595, 2018.

Xu Zhang, Svebor Karaman, and Shih-Fu Chang. Detecting and simulating artifacts in gan fake images. In *IEEE International Workshop on Information Forensics and Security*, pp. 1–6. IEEE, 2019.

Jun-Yan Zhu, Taesung Park, Phillip Isola, and Alexei A Efros. Unpaired image-to-image translation using cycle-consistent adversarial networks. In *Proceedings of the IEEE International Conference on Computer Vision*, pp. 2223–2232, 2017.

Mingjian Zhu, Hanting Chen, Qiangyu Yan, Xudong Huang, Guanyu Lin, Wei Li, Zhijun Tu, Hailin Hu, Jie Hu, and Yunhe Wang. Genimage: A million-scale benchmark for detecting ai-generated image. *Advances in Neural Information Processing Systems*, 36:77771–77782, 2023.

Appendix

A More Analysis of Captioning Models

In Section 4.5, we analyzed the impact of different captioning models on detection performance. To further examine the differences between BLIP (Li et al., 2022) and LLaVA-NeXT (Liu et al., 2024), we present additional analysis based on LPIPS scores (Zhang et al., 2018) and visualizations.

LPIPS-Based Semantic Shift Analysis We measured the LPIPS scores between original images and their caption-guided reconstructions. Figure 7a shows the average LPIPS scores of real and fake images in each subset of the GenImage dataset (Zhu et al., 2023) under two conditions: (1) using captions generated by BLIP, and (2) using captions generated by LLaVA-NeXT. In both cases, real images consistently yield higher LPIPS scores than fake images, suggesting that caption-guided reconstruction serves as a reliable cue for detection. However, as shown in Table 7b, the LPIPS score gap between real and fake images, denoted as Δ in Eq. 7, is smaller with LLaVA-NeXT than with BLIP, which explains the slightly lower performance reported in Table 5.

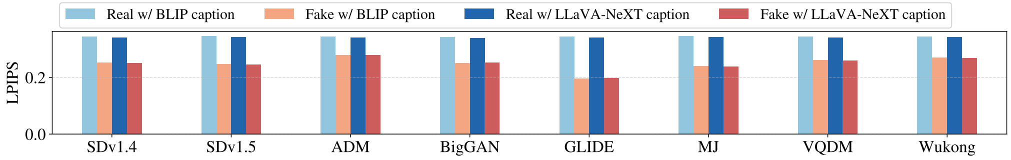

(a) Average LPIPS scores between original images and their reconstructions.

Δ	SDv1.4	SDv1.5	ADM	BigGAN	GLIDE	MJ	VQDM	Wukong
w/ BLIP caption	0.091	0.098	0.065	0.091	0.147	0.105	0.082	0.076
w/ LLaVA-NeXT caption	0.090	0.096	0.062	0.088	0.144	0.103	0.080	0.073

(b) Δ values measuring the LPIPS score gap between real and fake images.

Figure 7: Semantic shift analysis based on LPIPS scores (Zhang et al., 2018). Higher scores indicate lower similarity between the original and reconstructed images. Images are reconstructed under two conditions: (1) using captions generated by BLIP (Li et al., 2022), and (2) using captions generated by LLaVA-NeXT (Liu et al., 2024)

Method	JPEG (QF=90)	JPEG (QF=80)	JPEG (QF=70)	Scale (0.75)	Scale (1.25)
GramNet (Liu et al., 2020)	71.22	71.02	71.22	69.89	66.31
Conv-B (Liu et al., 2022)	71.91	71.57	71.42	75.30	75.28
UnivFD (Ojha et al., 2023)	73.24	70.42	69.75	75.96	73.99
DIRE (Wang et al., 2023)	52.79	50.65	50.34	51.94	53.77
DE-FAKE (Sha et al., 2023)	71.00	70.88	70.44	72.33	71.88
NPR (Tan et al., 2024)	69.44	70.94	70.77	71.27	71.20
AIDE (Yan et al., 2025)	57.22	58.50	60.45	83.13	83.79
DRCT (Chen et al., 2024)	80.97	78.06	76.18	79.51	74.75
SARE (ours)	85.64	82.72	79.14	87.60	82.74

Table 7: Accuracy (ACC, %) performance of robustness evaluation on the GenImage (Zhu et al., 2023) dataset. QF denotes JPEG quality factor. For NPR (Tan et al., 2024) and AIDE (Yan et al., 2025), the publicly released checkpoints are used.

Method	JPEG (QF=90)	JPEG (QF=80)	JPEG (QF=70)	Scale (0.75)	Scale (1.25)
GramNet (Liu et al., 2020)	80.12	81.71	81.15	69.47	69.32
Conv-B (Liu et al., 2022)	90.53	90.17	90.43	94.15	96.90
UnivFD (Ojha et al., 2023)	85.31	82.53	81.08	85.48	82.05
DIRE (Wang et al., 2023)	70.83	63.44	59.23	78.92	80.61
DE-FAKE (Sha et al., 2023)	79.89	79.02	77.96	81.09	78.10
NPR (Tan et al., 2024)	75.23	76.54	77.09	90.87	92.12
AIDE (Yan et al., 2025)	75.23	78.12	80.66	96.28	96.00
DRCT (Chen et al., 2024)	88.89	86.18	84.05	89.29	87.93
SARE (ours)	94.33	93.10	89.68	94.97	92.77

Table 8: AUC (%) performance of robustness evaluation on the GenImage (Zhu et al., 2023) dataset. QF denotes JPEG quality factor. For NPR (Tan et al., 2024) and AIDE (Yan et al., 2025), the publicly released checkpoints are used.

Additional Visualizations Figures 9–12 present real and fake images from the GenImage dataset and their reconstructions guided by captions from BLIP and LLaVA-NeXT. To ensure a fair comparison, real and fake images are selected from the same ImageNet class label. The visualizations show that real images typically undergo larger semantic shifts than fake images during caption-guided reconstruction with both captioning models. In some real image cases, however, the detailed descriptions provided by LLaVA-NeXT yield reconstructions that remain relatively closer to the original input, whereas the concise captions generated by BLIP tend to produce larger shifts.

B Additional Ablation Study

Influence of *Strength* Parameter To evaluate the influence of the *strength* parameter on detection performance, we conducted an ablation study on the GenImage dataset by varying the *strength* value from 0.3 to 0.9. Figure 8 shows the accuracy and AUC performance for each *strength* value. The results demonstrate that the model maintains stable performance across all values. In particular, the highest accuracy is obtained at *strength* = 0.5, while the best AUC is achieved at *strength* = 0.7.

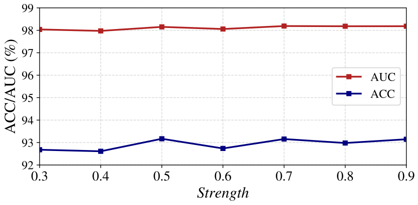

Figure 8: Ablation study on the *strength* parameter conducted on the GenImage dataset (Zhu et al., 2023).

C LLM Usage

Large language models (LLMs) were used solely for polishing the writing of this paper.

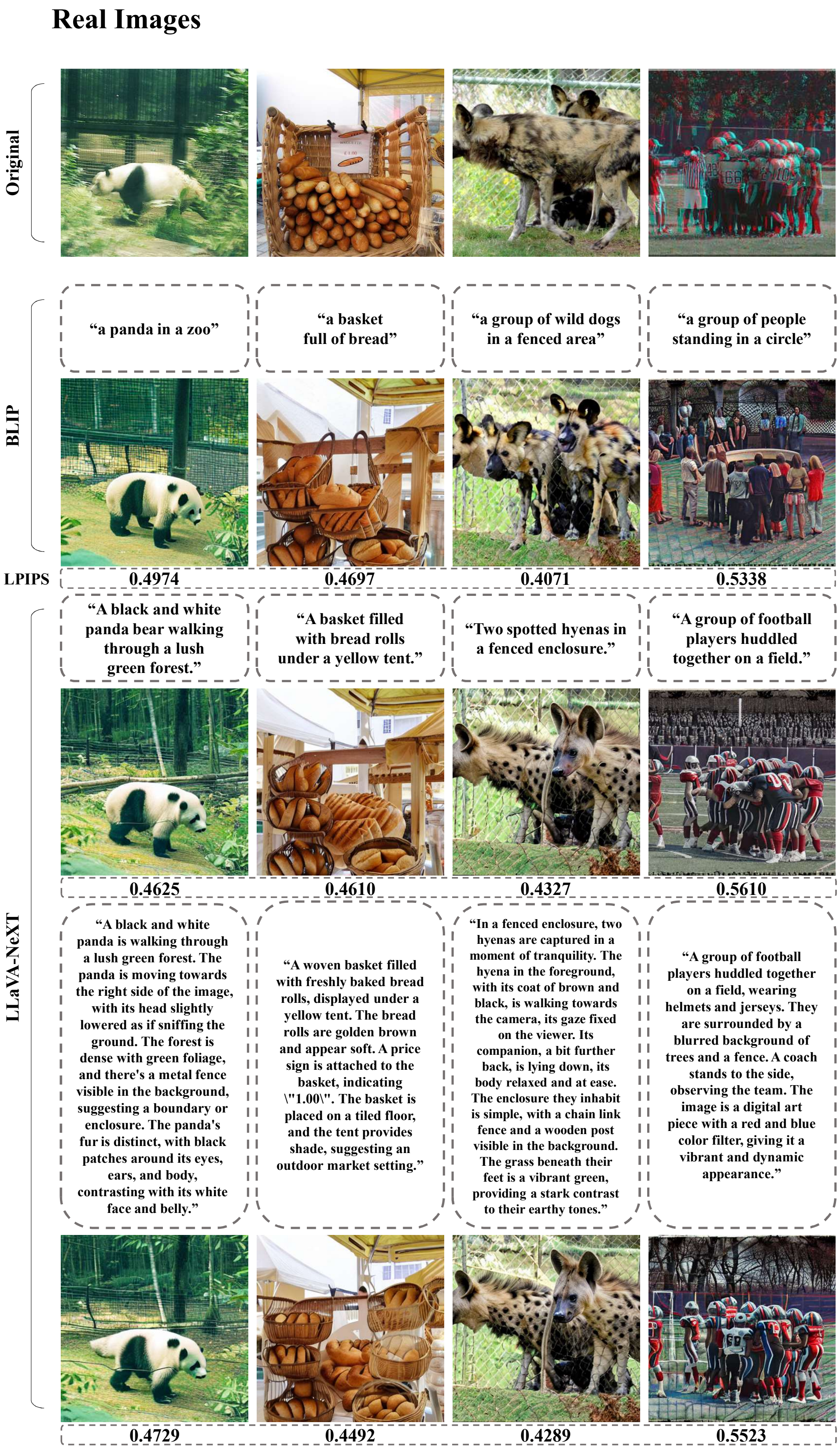

"a panda in a zoo"

"a basket full of bread"

"a group of wild dogs in a fenced area"

"a group of people standing in a circle"

"A black and white panda bear walking through a lush green forest."

"A basket filled with bread rolls under a yellow tent."

"Two spotted hyenas in a fenced enclosure."

"A group of football players huddled together on a field."

"A black and white panda is walking through a lush green forest. The panda is moving towards the right side of the image, with its head slightly lowered as if sniffing the ground. The forest is dense with green foliage, and there's a metal fence visible in the background, suggesting a boundary or enclosure. The panda's fur is distinct, with black patches around its eyes, ears, and body, contrasting with its white face and belly."

"A woven basket filled with freshly baked bread rolls, displayed under a yellow tent. The bread rolls are golden brown and appear soft. A price sign is attached to the basket, indicating \"1.00\". The basket is placed on a tiled floor, and the tent provides shade, suggesting an outdoor market setting."

"In a fenced enclosure, two hyenas are captured in a moment of tranquility. The hyena in the foreground, with its coat of brown and black, is walking towards the camera, its gaze fixed on the viewer. Its companion, a bit further back, is lying down, its body relaxed and at ease. The enclosure they inhabit is simple, with a chain link fence and a wooden post visible in the background. The grass beneath their feet is a vibrant green, providing a stark contrast to their earthy tones."

"A group of football players huddled together on a field, wearing helmets and jerseys. They are surrounded by a blurred background of trees and a fence. A coach stands to the side, observing the team. The image is a digital art piece with a red and blue color filter, giving it a vibrant and dynamic appearance."

Figure 9: Real images from the GenImage dataset (Zhu et al., 2023) with captions from BLIP (Li et al., 2022) and LLaVA-NeXT (Liu et al., 2024), their corresponding reconstructions, and LPIPS scores. For LLaVA-NeXT, we used the prompts "Brief description within 50 words." and "Detailed description within 80 words."

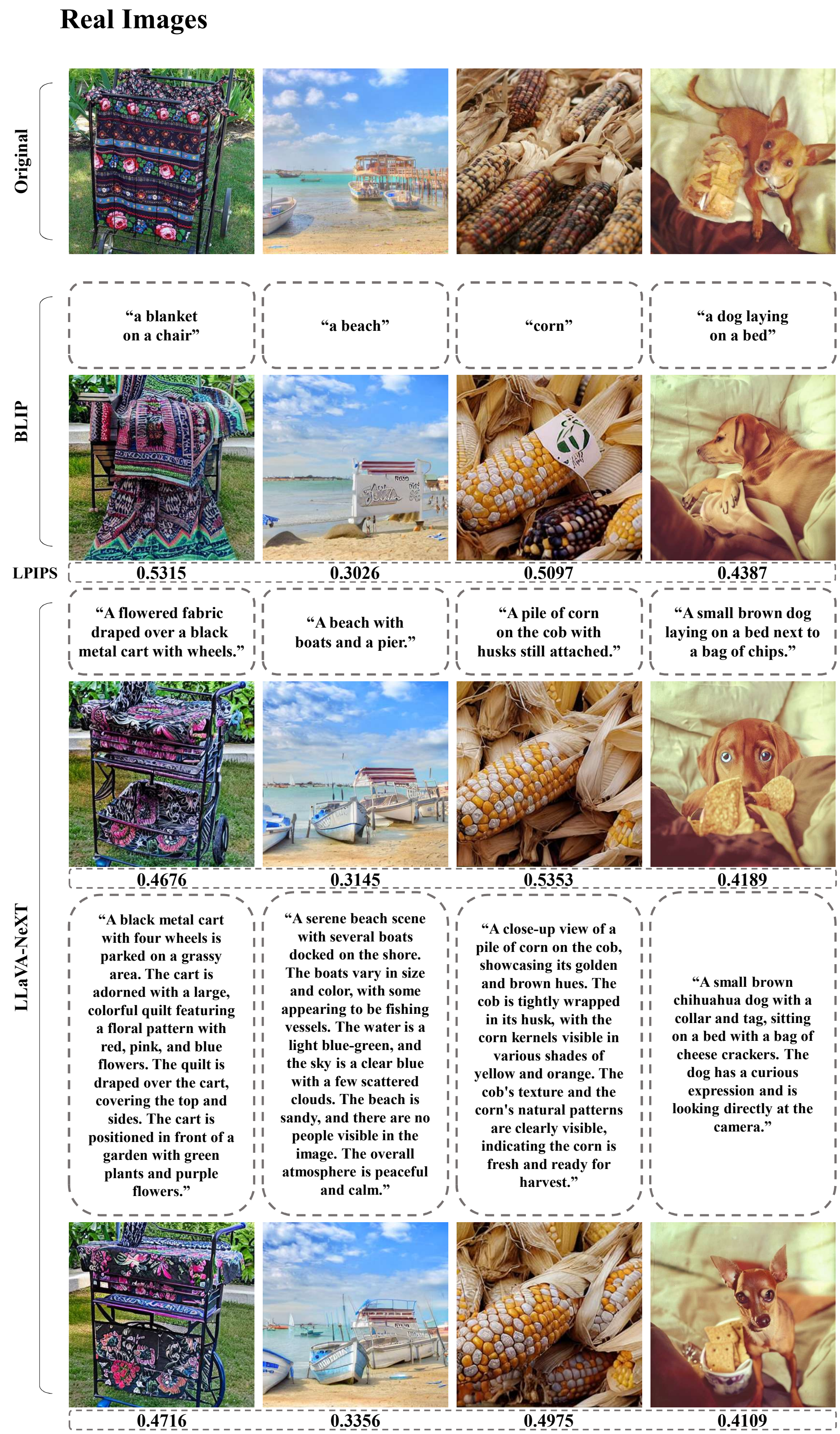

“a blanket on a chair”

“a beach”

“corn”

“a dog laying on a bed”

“A flowered fabric draped over a black metal cart with wheels.”

“A beach with boats and a pier.”

“A pile of corn on the cob with husks still attached.”

“A small brown dog laying on a bed next to a bag of chips.”

“A black metal cart with four wheels is parked on a grassy area. The cart is adorned with a large, colorful quilt featuring a floral pattern with red, pink, and blue flowers. The quilt is draped over the cart, covering the top and sides. The cart is positioned in front of a garden with green plants and purple flowers.”

“A serene beach scene with several boats docked on the shore. The boats vary in size and color, with some appearing to be fishing vessels. The water is a light blue-green, and the sky is a clear blue with a few scattered clouds. The beach is sandy, and there are no people visible in the image. The overall atmosphere is peaceful and calm.”

“A close-up view of a pile of corn on the cob, showcasing its golden and brown hues. The cob is tightly wrapped in its husk, with the corn kernels visible in various shades of yellow and orange. The cob's texture and the corn's natural patterns are clearly visible, indicating the corn is fresh and ready for harvest.”

“A small brown chihuahua dog with a collar and tag, sitting on a bed with a bag of cheese crackers. The dog has a curious expression and is looking directly at the camera.”

Figure 10: Real images from the GenImage dataset (Zhu et al., 2023) with captions from BLIP (Li et al., 2022) and LLaVA-NeXT (Liu et al., 2024), their corresponding reconstructions, and LPIPS scores. For LLaVA-NeXT, we used the prompts “Brief description within 50 words.” and “Detailed description within 80 words.”

Fake Images

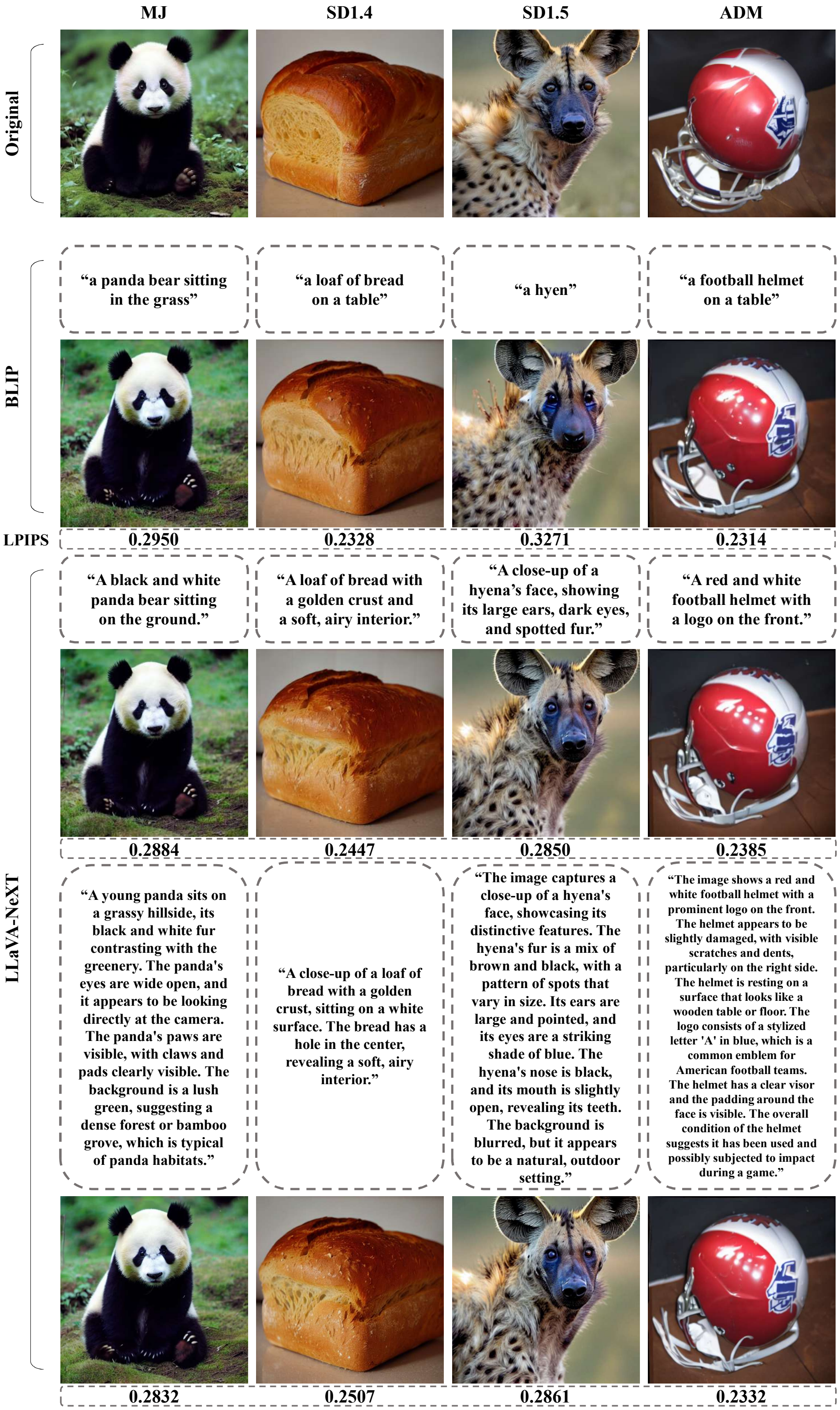

“a panda bear sitting in the grass”

“a loaf of bread on a table”

“a hyen”

“a football helmet on a table”

“A black and white panda bear sitting on the ground.”

“A loaf of bread with a golden crust and a soft, airy interior.”

“A close-up of a hyena’s face, showing its large ears, dark eyes, and spotted fur.”

“A red and white football helmet with a logo on the front.”

“A young panda sits on a grassy hillside, its black and white fur contrasting with the greenery. The panda's eyes are wide open, and it appears to be looking directly at the camera. The panda's paws are visible, with claws and pads clearly visible. The background is a lush green, suggesting a dense forest or bamboo grove, which is typical of panda habitats.”

“A close-up of a loaf of bread with a golden crust, sitting on a white surface. The bread has a hole in the center, revealing a soft, airy interior.”

“The image captures a close-up of a hyena's face, showcasing its distinctive features. The hyena's fur is a mix of brown and black, with a pattern of spots that vary in size. Its ears are large and pointed, and its eyes are a striking shade of blue. The hyena's nose is black, and its mouth is slightly open, revealing its teeth. The background is blurred, but it appears to be a natural, outdoor setting.”

“The image shows a red and white football helmet with a prominent logo on the front. The helmet appears to be slightly damaged, with visible scratches and dents, particularly on the right side. The helmet is resting on a surface that looks like a wooden table or floor. The logo consists of a stylized letter 'A' in blue, which is a common emblem for American football teams. The helmet has a clear visor and the padding around the face is visible. The overall condition of the helmet suggests it has been used and possibly subjected to impact during a game.”

Figure 11: Fake images from the GenImage dataset (Zhu et al., 2023) with captions from BLIP (Li et al., 2022) and LLaVA-NeXT (Liu et al., 2024), their corresponding reconstructions, and LPIPS scores. For LLaVA-NeXT, we used the prompts “Brief description within 50 words.” and “Detailed description within 80 words.”

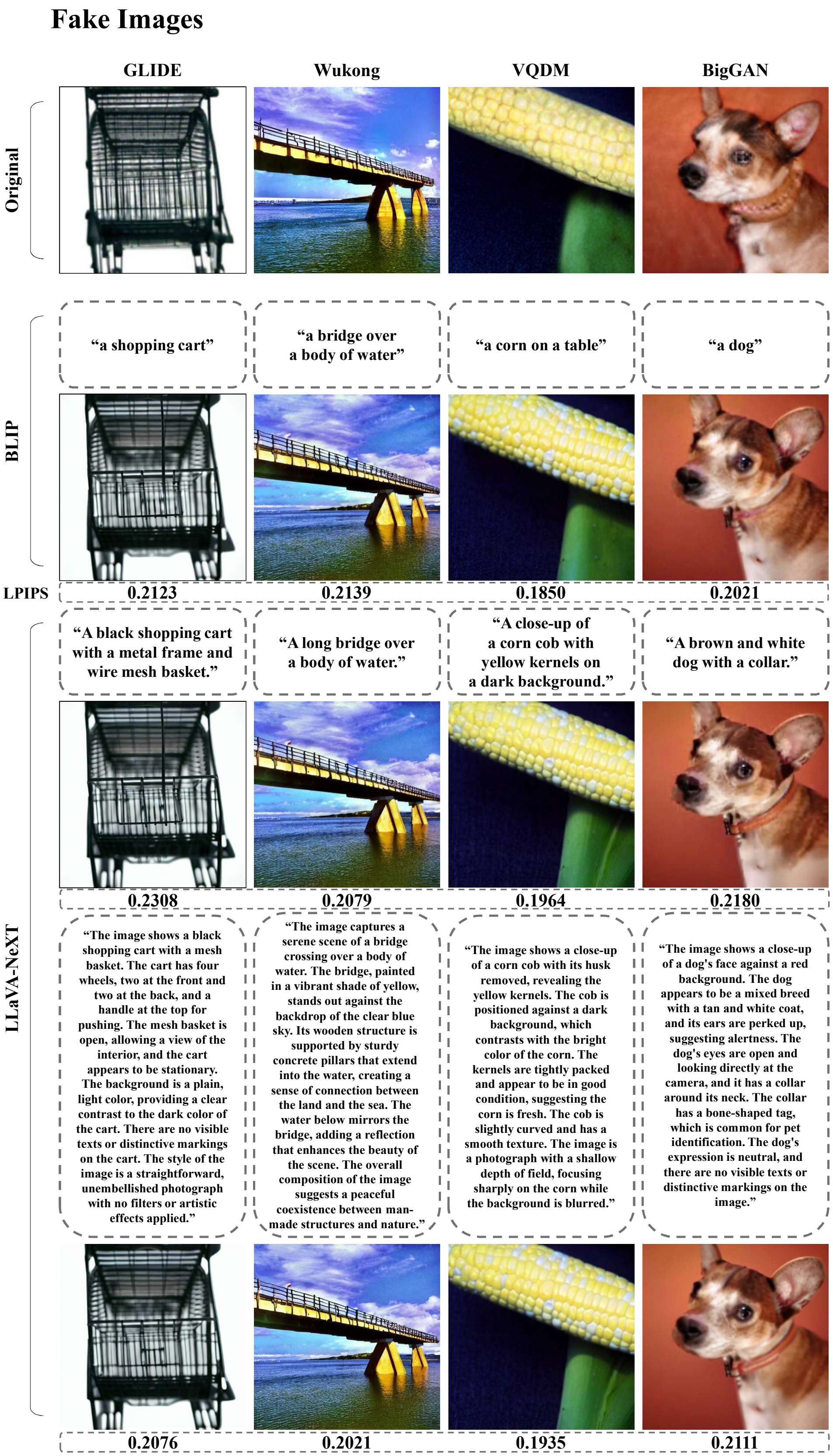

"a shopping cart"

"a bridge over a body of water"

"a corn on a table"

"a dog"

"A black shopping cart with a metal frame and wire mesh basket."

"A long bridge over a body of water."

"A close-up of a corn cob with yellow kernels on a dark background."

"A brown and white dog with a collar."

"The image shows a black shopping cart with a mesh basket. The cart has four wheels, two at the front and two at the back, and a handle at the top for pushing. The mesh basket is open, allowing a view of the interior, and the cart appears to be stationary. The background is a plain, light color, providing a clear contrast to the dark color of the cart. There are no visible texts or distinctive markings on the cart. The style of the image is a straightforward, unembellished photograph with no filters or artistic effects applied."

"The image captures a serene scene of a bridge crossing over a body of water. The bridge, painted in a vibrant shade of yellow, stands out against the backdrop of the clear blue sky. Its wooden structure is supported by sturdy concrete pillars that extend into the water, creating a sense of connection between the land and the sea. The water below mirrors the bridge, adding a reflection that enhances the beauty of the scene. The overall composition of the image suggests a peaceful coexistence between man-made structures and nature."

"The image shows a close-up of a corn cob with its husk removed, revealing the yellow kernels. The cob is positioned against a dark background, which contrasts with the bright color of the corn. The kernels are tightly packed and appear to be in good condition, suggesting the corn is fresh. The cob is slightly curved and has a smooth texture. The image is a photograph with a shallow depth of field, focusing sharply on the corn while the background is blurred."

"The image shows a close-up of a dog's face against a red background. The dog appears to be a mixed breed with a tan and white coat, and its ears are perked up, suggesting alertness. The dog's eyes are open and looking directly at the camera, and it has a collar around its neck. The collar has a bone-shaped tag, which is common for pet identification. The dog's expression is neutral, and there are no visible texts or distinctive markings on the image."

Figure 12: Fake images from the GenImage dataset (Zhu et al., 2023) with captions from BLIP (Li et al., 2022) and LLaVA-NeXT (Liu et al., 2024), their corresponding reconstructions, and LPIPS scores. For LLaVA-NeXT, we used the prompts "Brief description within 50 words." and "Detailed description within 80 words."

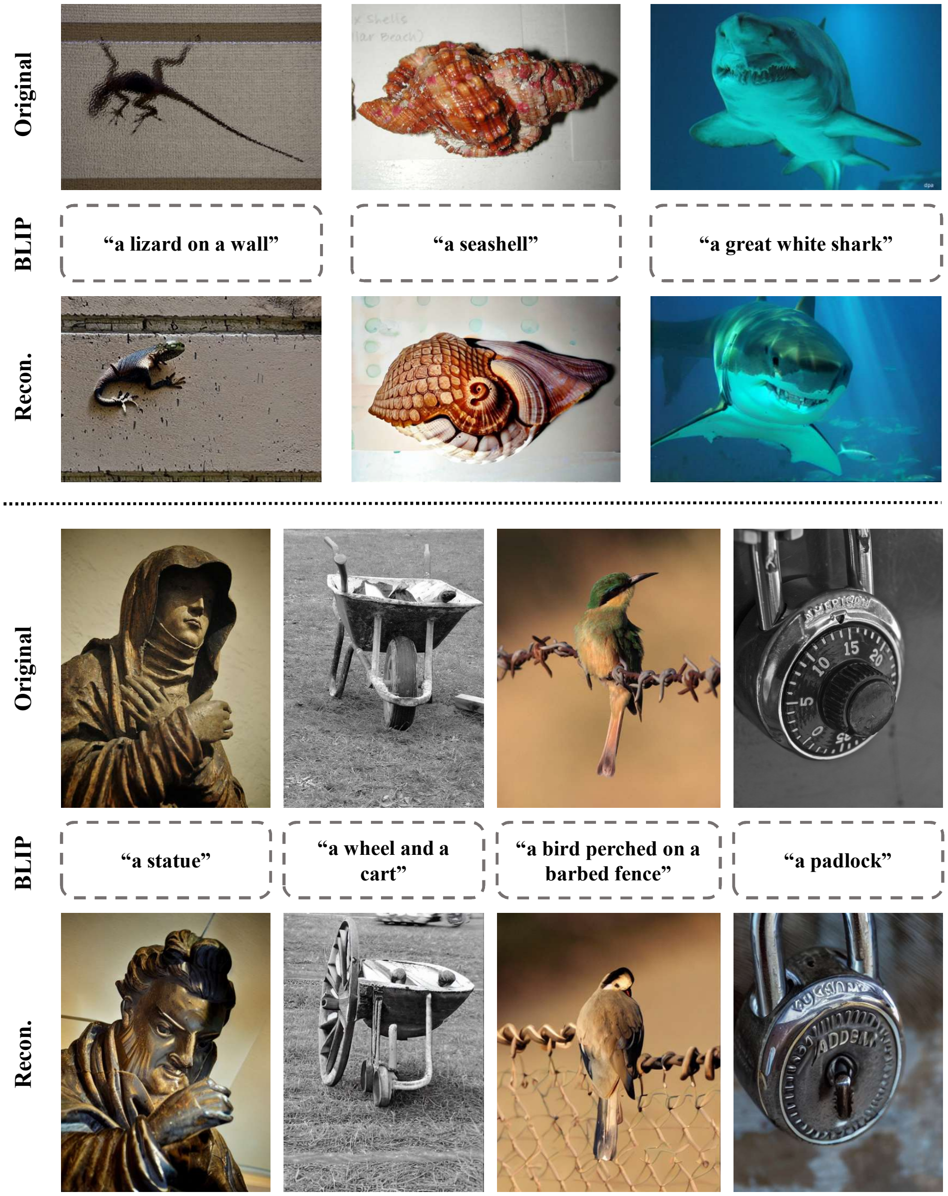

Figure 13: Single object real images from the GenImage dataset (Zhu et al., 2023) with captions from BLIP (Li et al., 2022) and their reconstructions.

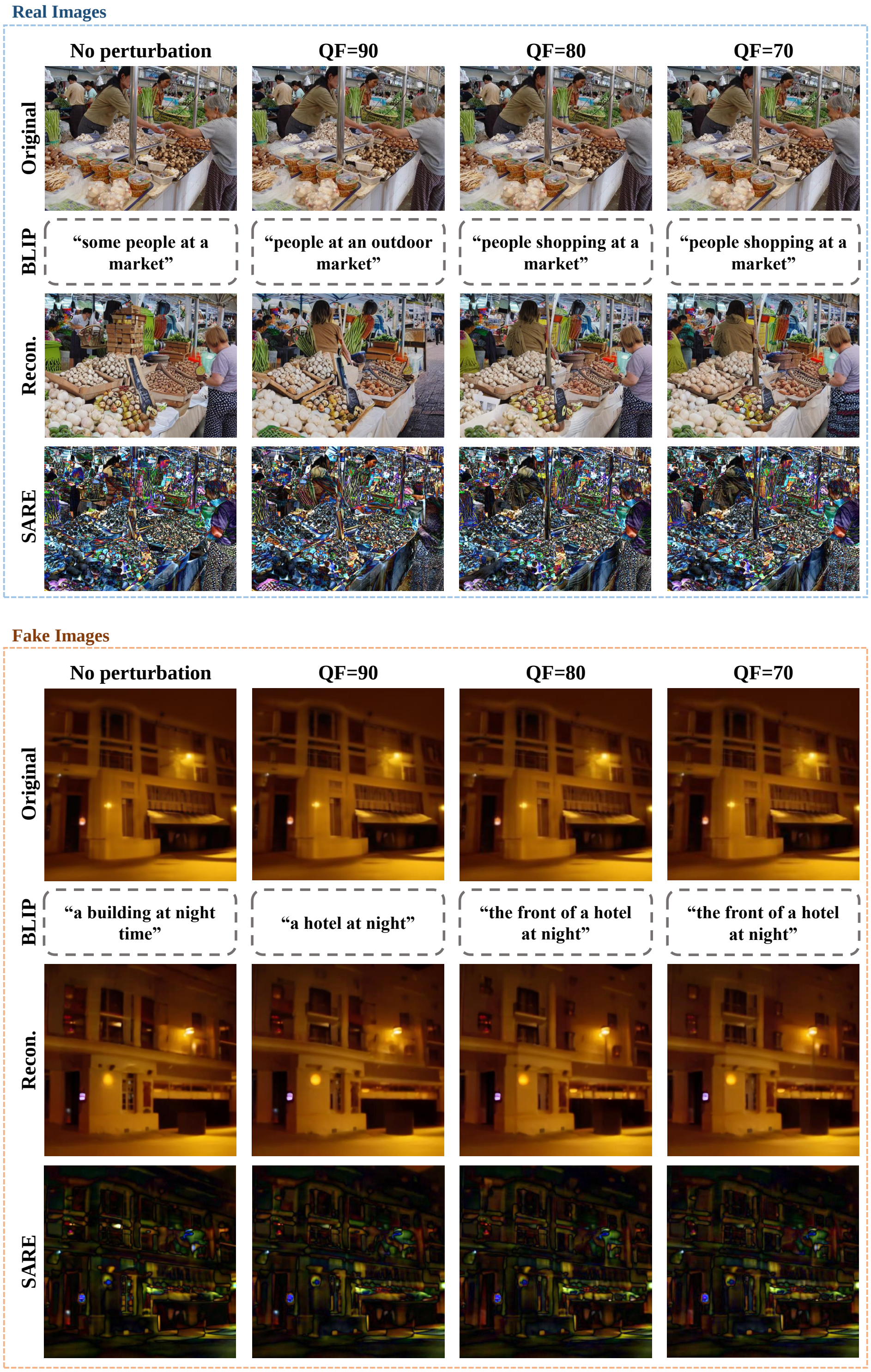
Real Images
No perturbation
QF=90
QF=80
QF=70
Original
BLIP
"some people at a market"
"people at an outdoor market"
"people shopping at a market"
"people shopping at a market"
Recon.
SARE
Fake Images
No perturbation
QF=90
QF=80
QF=70
Original
BLIP
"a building at night time"
"a hotel at night"
"the front of a hotel at night"
"the front of a hotel at night"
Recon.
SARE

Figure 14: Real and fake images from the GenImage (Zhu et al., 2023) dataset under different levels of JPEG compression (QF = 90, 80, 70), along with their captions generated by BLIP (Li et al., 2022) and caption-guided reconstructions.

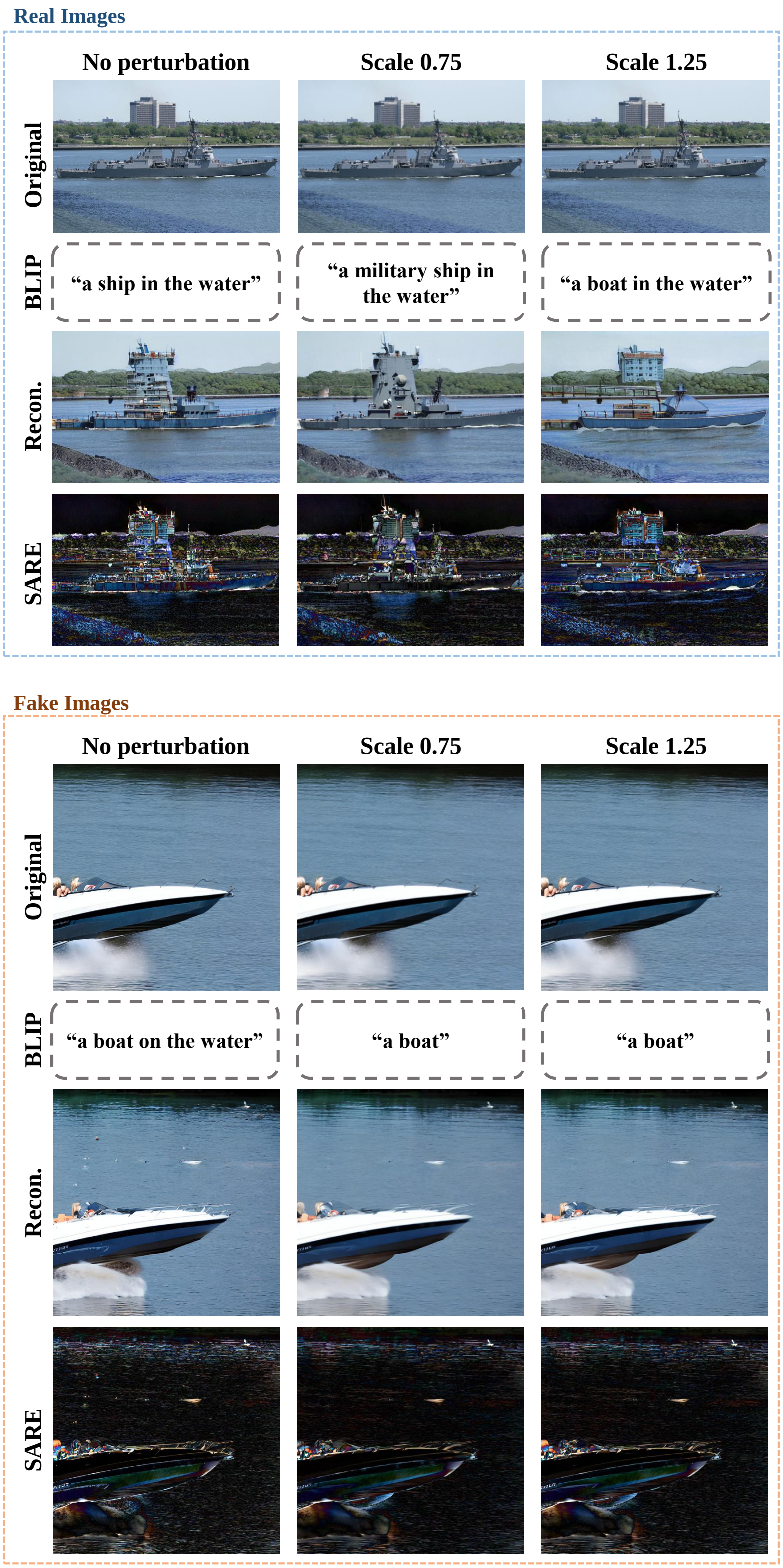

Figure 15: Real and fake images from the GenImage (Zhu et al., 2023) dataset under different levels of scaling (0.75, 1.25), along with their captions generated by BLIP (Li et al., 2022) and caption-guided reconstructions.

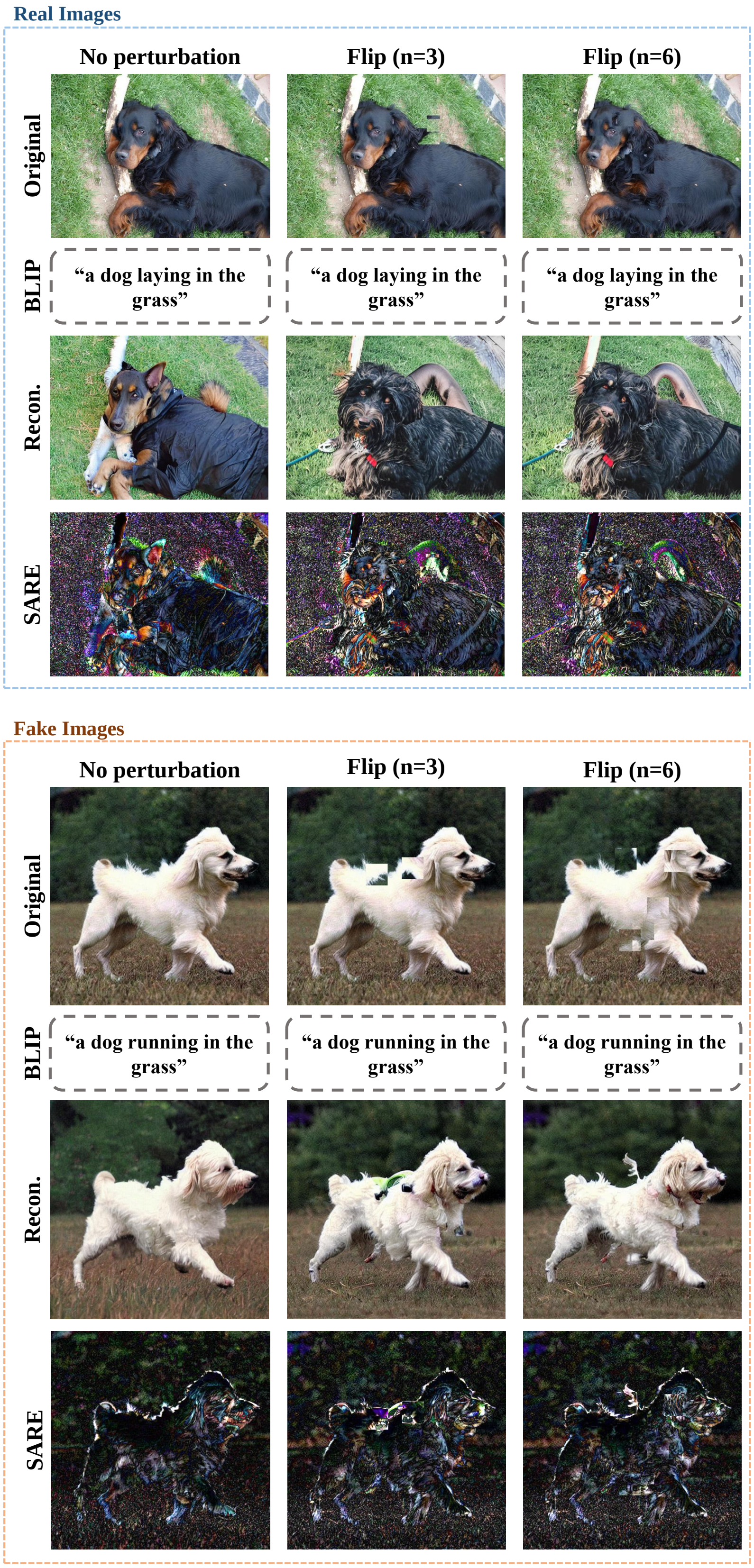
Real Images
No perturbation
Flip (n=3)
Flip (n=6)
Original
BLIP
"a dog laying in the grass"
"a dog laying in the grass"
"a dog laying in the grass"
Recon.
SARE
Fake Images
No perturbation
Flip (n=3)
Flip (n=6)
Original
BLIP
"a dog running in the grass"
"a dog running in the grass"
"a dog running in the grass"
Recon.
SARE

Figure 16: Real and fake images from the GenImage (Zhu et al., 2023) dataset under flip perturbations (3 or 6 regions per image), along with their captions generated by BLIP (Li et al., 2022) and caption-guided reconstructions.

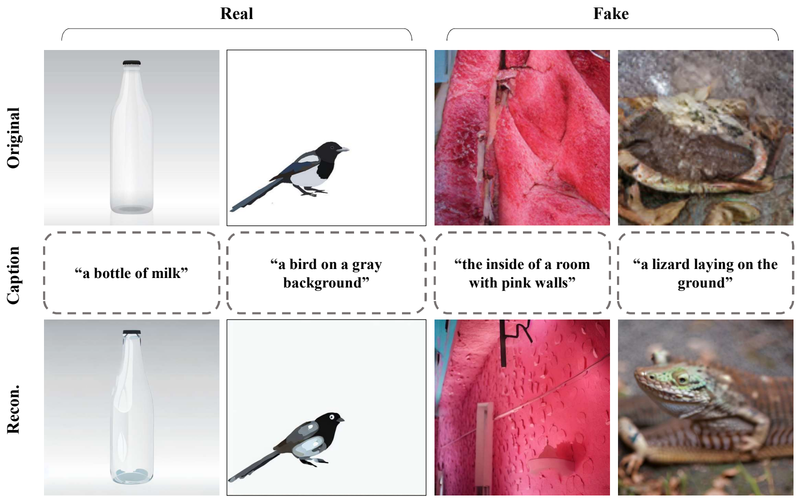
Real
Fake
Original
Caption
Recon.
“a bottle of milk”
“a bird on a gray background”
“the inside of a room with pink walls”
“a lizard laying on the ground”

Figure 17: Failure cases of caption-guided reconstructions for real and fake images from the GenImage (Zhu et al., 2023) dataset.

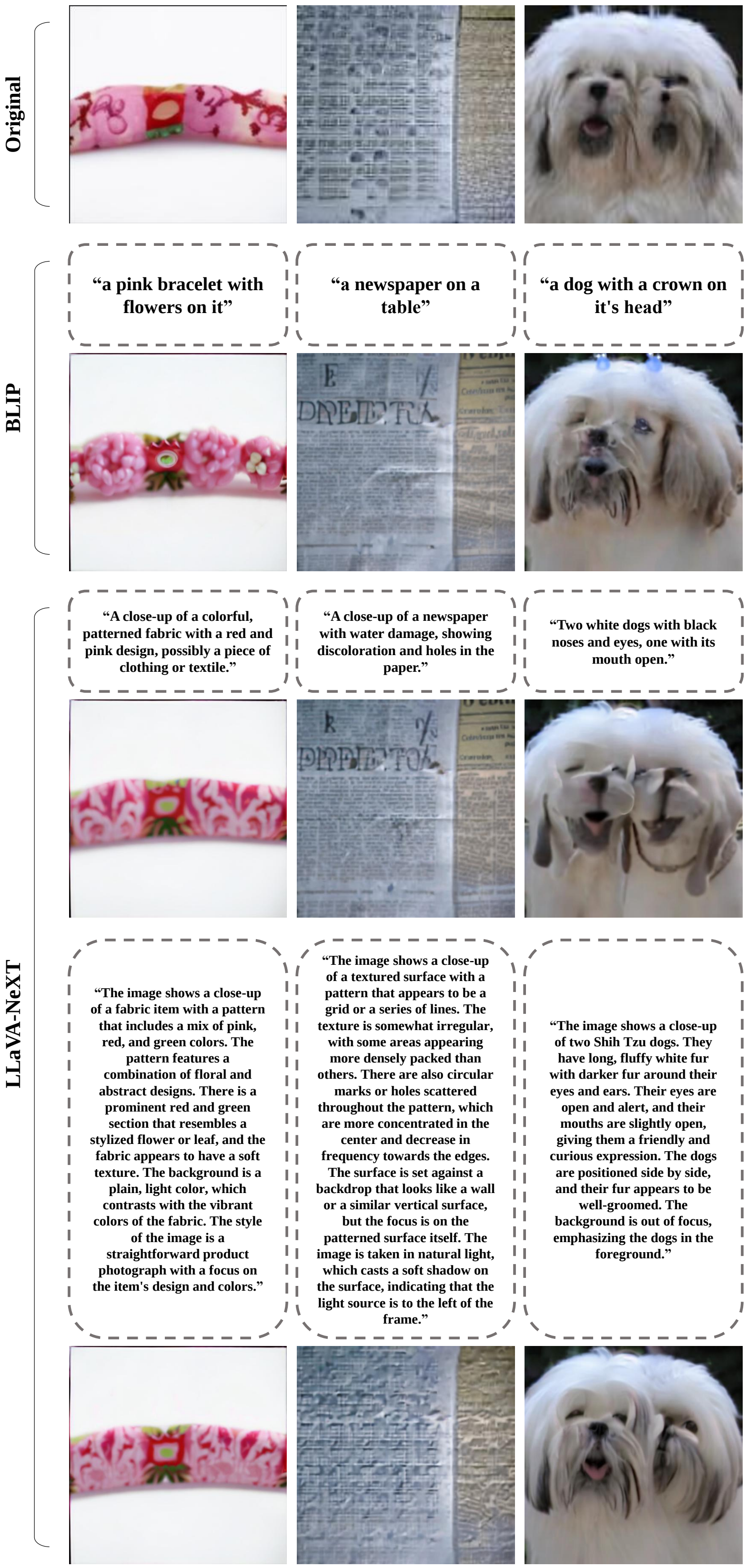

"a pink bracelet with flowers on it"

"a newspaper on a table"

"a dog with a crown on it's head"

"A close-up of a colorful, patterned fabric with a red and pink design, possibly a piece of clothing or textile."

"A close-up of a newspaper with water damage, showing discoloration and holes in the paper."

"Two white dogs with black noses and eyes, one with its mouth open."

"The image shows a close-up of a fabric item with a pattern that includes a mix of pink, red, and green colors. The pattern features a combination of floral and abstract designs. There is a prominent red and green section that resembles a stylized flower or leaf, and the fabric appears to have a soft texture. The background is a plain, light color, which contrasts with the vibrant colors of the fabric. The style of the image is a straightforward product photograph with a focus on the item's design and colors."

"The image shows a close-up of a textured surface with a pattern that appears to be a grid or a series of lines. The texture is somewhat irregular, with some areas appearing more densely packed than others. There are also circular marks or holes scattered throughout the pattern, which are more concentrated in the center and decrease in frequency towards the edges. The surface is set against a backdrop that looks like a wall or a similar vertical surface, but the focus is on the patterned surface itself. The image is taken in natural light, which casts a soft shadow on the surface, indicating that the light source is to the left of the frame."

"The image shows a close-up of two Shih Tzu dogs. They have long, fluffy white fur with darker fur around their eyes and ears. Their eyes are open and alert, and their mouths are slightly open, giving them a friendly and curious expression. The dogs are positioned side by side, and their fur appears to be well-groomed. The background is out of focus, emphasizing the dogs in the foreground."

Figure 18: Fake images containing artifacts and distortions from the GenImage (Zhu et al., 2023) dataset and their caption-guided reconstructions.